Supplementary Information (SI) for Catalysis Science & Technology.
This journal is © The Royal Society of Chemistry 2024

Supplementary Material

Enhancing photocatalytic N_2 fixation under ambient conditions through Zn vacancy-mediated engineering in $Cd_{0.5}Zn_{0.5}S$

Xiangju Ye,[a] Qiaoqiao Zhang,[a,b] Miaomiao Jiang,[a] Zhenzhen Hui,[a] Errui Wang,[a] Shifu Chen[b*]

[a]College of Chemistry and Materials Engineering, Anhui Science and Technology University, Bengbu, Anhui 233030, P. R. China.

[b]College of Chemistry and Material Science, Huaibei Normal University, Huaibei, 235000, P. R. China.

*Corresponding author, Tel: +86-561-3806611, Fax: +86-561-3806611. E-mail: chshifu@chnu.edu.cn

Experimental section

Materials

All chemical reagents were purchased from Aladdin Reagent Company and used as received without additional purification or treatment. Homemade deionized water in our laboratory was used in all experiments.

Characterization of samples

X-ray diffraction patterns were performed on a Bruker D8 Advance diffractometer with Cu-Kα radiation (λ= 0.154056 nm) and a scanning speed of 10 °/min to obtain the crystal phase of the samples. The element contents of $Cd_{0.5}Zn_{0.5}S$ photocatalysts were detected by inductively coupled plasma-mass spectrometry (ICP-MS, Agilent 7700s). UV-Vis diffuse reflectance spectra (UV-Vis DRS) measurements were analyzed by a Shimadzu UV3600 UV-Vis-NIR spectrometer using $BaSO_4$ as a reflectance standard. X-ray photoelectron spectroscopy (XPS) measurements were carried out on a Kratos Axis Supra instrument using monochromatic Al Kα radiation (1486.7 eV, 150 W). The binding energy values were calibrated using the contaminant carbon (C1s = 284.6 eV). The Brunauer-Emment-Teller (BET) surface areas were carried out by N_2 adsorption-desorption at 77.3 K using a Micromeritics ASAP 2460 instrument. The morphologies and microstructures of the photocatalysts were examined using a JEOL7800 F scanning electron microscopy (SEM). Transmission electron microscopy (TEM) and high-resolution transmission electron microscopy (HRTEM) images were collected using a FEI-G2 transmission electron microscope with an acceleration voltage of 200 kV. Electron paramagnetic resonance (EPR) measurements were carried out on a Bruker model A300 spectrometer with a 300 W Xe lamp (Beijing China Education Au-light Co., Ltd) equipped with a cut-off filter (λ≥420 nm) as a visible light source. Electrochemical analysis was performed on a CHI 660D electrochemical workstation (Shanghai Chenhua) using a standard three-electrode quartz cell. To prepare the working electrode, a catalyst powder was

deposited on the tin-doped tin oxide (FTO) substrate. 5 mg catalyst powder was suspended in 5 mL of deionized water and the mixture was sonicated for 30 minutes. Then, 200 μL or more of the slurry was coated on the FTO glass, which was used as a working electrode. A 300 W Xenon lamp (CEL-HXF300E7, Beijing China Education Au-light Co., Ltd) equipped with a 420 nm cutoff filter ($\lambda \geqslant 420$ nm) was applied as a visible light source. Mott-Schottky (M-S) experiments of the resulting samples were analyzed in the potential range of -1.0 to 0.1 V with the amplitude of 0.01 at a constant frequency of 1000 Hz, with the electrolyte system consisting of 0.1 M KCl and 0.1 M $K_3[Fe(CN)_6]/K_4[Fe(CN)_6]$ solution. During the photocurrent experiments, the electrolyte system is composed of 0.2 M Na_2SO_4 solution.

Computational method

The study used VASP to perform density functional theory calculations with projector augmented wave [1,2]. Electron spin polarization were considered in all calculations. The Perdew-Burke-Ernzerhof functional was employed for exchange-correlation effects [3], while DFT+D3 was used for handling weak interactions [4]. The cut-off energy for the plane-wave basis was 450 eV. K-points were 2×2×2 in the Brillouin zone. Energy and maximum stress were converged to 10^{-5} eV and 0.02 eV/Å, respectively.

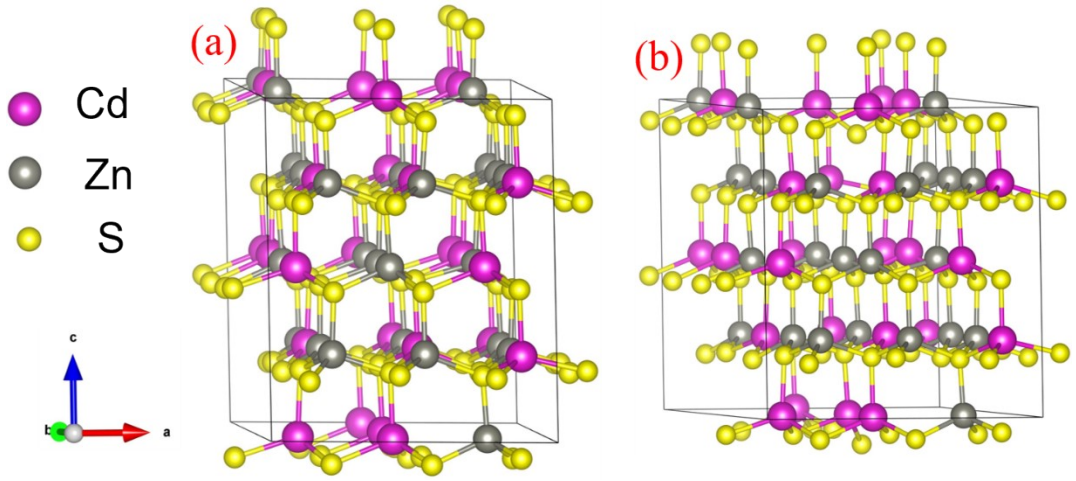

Fig. S1. Constructed $Cd_{0.5}Zn_{0.5}S$ (a) and V_{Zn}-$Cd_{0.5}Zn_{0.5}S$ (b) crystal structures.

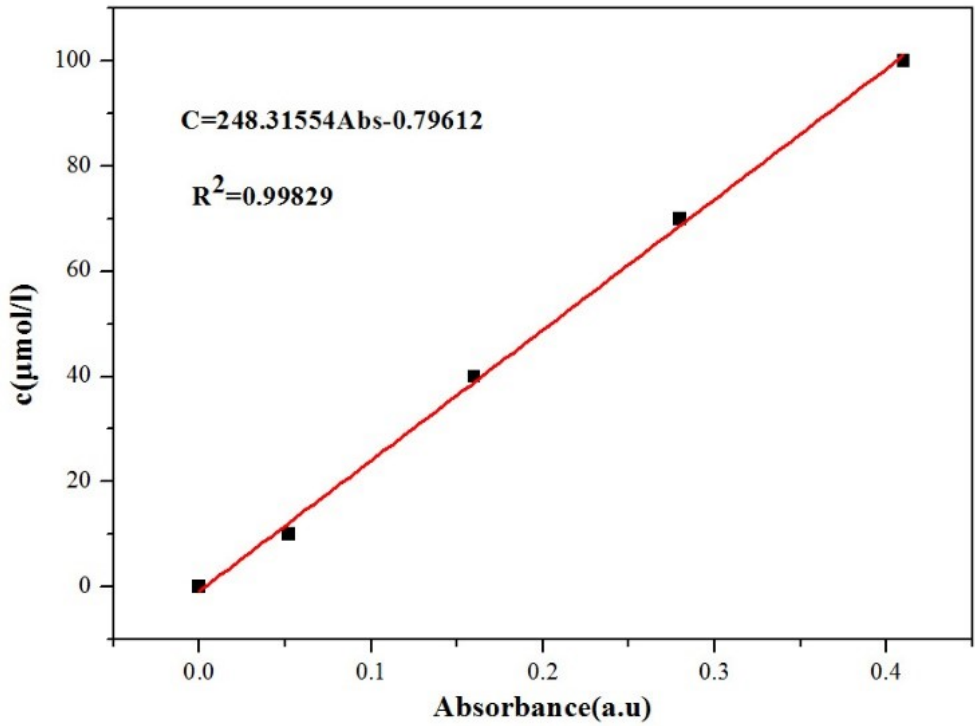

Fig. S2. The standard calibration curve for colorimetric NH_4^+ assay obtained by a Nessler's reagent colorimetric method.

Table S1 The comparison the photocatalytic performance in N_2 fixation of various materials with our prepared $Cd_{0.5}Zn_{0.5}S$ samples.

photocatalyst	Light source and wavelength	Catalyst dosage	ammonia evolution	Reference
$Cd_{0.5}Zn_{0.5}S$	300 W Xe lamp (λ≥ 420 nm)	30 mg	1465 μmol·L^{-1}·h^{-1}	This work
$Ni_2P/Cd_{0.5}Zn_{0.5}S$	300 W Xe lamp (λ≥ 400 nm)	20 mg	101.5 μmol·L^{-1}·h^{-1}	[5]
V_{Zn}-$Zn_3In_2S_6$	300 W Xe lamp (λ≥ 420 nm)	30 mg	88.8 mg·L^{-1} ·g_{cat}^{-1}·h^{-1}	[6]
Ru/BiOBr-NF	300 W Xe lamp (λ= 200-800 nm)	10 mg	121.97 μmol·g^{-1}·h^{-1}	[7]
MIL-68(InFe) MOF	300 W Xe lamp (λ≥ 320 nm)	5 mg	30.8 μmol·g^{-1}·h^{-1}	[8]
NVs-g-C_3N_4	300 W Xe lamp (λ> 420 nm)	50 mg	1240 μmol·g_{cat}^{-1}·h^{-1}	[9]
$AuRu_X$	300 W Xe lamp (λ= 200-800 nm)	0.2 mg	101.4 μmol·g^{-1}·h^{-1}	[10]
Bi_5O_7Br-NT	300 W Xe lamp (λ> 400 nm)	25 mg	1.38 mmol·g^{-1}·h^{-1}	[11]
TiO_2 nanosheets	300 W Xe lamp (λ= 200-800 nm)	20 mg	78.9 μmol·g^{-1}·h^{-1}	[12]
Mo-doped $W_{18}O_{49}$	300 W Xe lamp (λ> 400 nm)	10 mg	195.5 μmol·g_{cat}^{-1}·h^{-1}	[13]
MoS_2/UiO-66$(SH)_2$	visible light (λ> 400 nm)	25 mg	54.08 μmol·g^{-1}·h^{-1}	[14]
COF4-Au	300 W Xe lamp	10 mg	427.9±18.7 μmol·g^{-1}·h^{-1}	[15]
g-C_3N_4-TiO_2	300 W Xe lamp (λ> 420 nm)	50 mg	~1.06 mmol·g^{-1}·h^{-1}	[16]
Cs(6)Ru(2)@ZrO_2	300 W Xe lamp	50 mg	5.1 mmol·g_{cat}^{-1}·h^{-1}	[17]

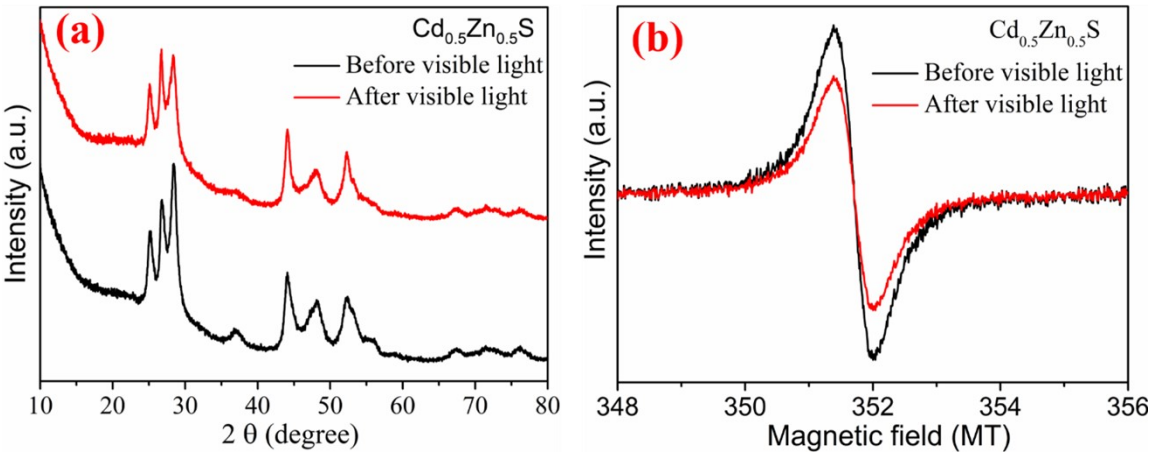

Fig. S3. XRD patterns (a) and EPR spectra (b) of the $Cd_{0.5}Zn_{0.5}S$ sample synthesized at 200 ℃ before and after visible light reaction.

Reference

[1] G. Kresse, J. Furthmüller, Efficient iterative schemes for ab initio total-energy calculations using a plane-wave basis set. Phys. Rev. B, 1996, 54, 11169.

[2] P. E. Blöchl, Projector augmented-wave method. Phys. Rev. B, 1994, 50, 17953-17979.

[3] J. P. Perdew, K. Burke, M. Ernzerhof, Generalized gradient approximation made simple. Phys. Rev. Lett., 1996, 77, 3865.

[4] S. Grimme, J. Antony, S. Ehrlich, H. Krieg, A consistent and accurate ab initio parametrization of density functional dispersion correction (DFT-D) for the 94 elements H-Pu, J. Chem. Phys., 2010, 132, 154104.

[5] L. Ye, C. Han, Z. Ma, Y. Leng, J. Li, X. Ji, D. Bi, H. Xie, Z. Huang, Ni_2P loading on $Cd_{0.5}Zn_{0.5}S$ solid solution for exceptional photocatalytic nitrogen fixation under visible light, Chem. Eng. J., 2017, 307, 311-318.

[6] H. Han, Y. Yang, J. Liu, X. Zheng, X. Wang, S. Meng, S. Zhang, X. Fu, S. Chen, Effect of Zn Vacancies in $Zn_3In_2S_6$ Nanosheets on boosting photocatalytic N_2 fixation, ACS Appl. Energy Mater., 2020, 3, 11, 11275-11284.

[7] Y. Xia, X. Xia, L. Chen, R. Liang, G. Yan, S. Liang, O defect anchored Ru on BiOBr with nanoconfined structure for catalytic N_2 fixation, Appl. Catal. B Environ. Energy, 2024, 349, 123859.

[8] C. Liu, M. Chen, Y. Chen, Q. Chen, J. Wu, S. Lin, L. Wu, J. C. Yu, Bimetallic MIL-68(InFe) MOF nanorods for biomimetic photocatalytic N_2 fixation, Chem. Eng. J., 2024, 498, 155646.

[9] G. Dong, W. Ho, C. Wang, Selective photocatalytic N_2 fixation dependent on g-C_3N_4 induced by nitrogen vacancies, J. Mater. Chem. A, 2015, 3, 23435-23441.
[10] C. Hu, X. Chen, J. Jin, Y. Han, S. Chen, H. Ju, J. Cai, Y. Qiu, C. Gao, C. Wang, Z. Qi, R. Long, L. Song, Z. Liu, Y. Xiong, Surface plasmon enabling nitrogen fixation in pure water through a dissociative mechanism under mild conditions, J. Am. Chem. Soc., 2019, 141, 7807-7814.
[11] S. Wang, X. Hai, X. Ding, K. Chang, Y. Xiang, X. Meng, Z. Yang, H. Chen, J. Ye, Light-switchable oxygen vacancies in ultrafine Bi_5O_7Br nanotubes for boosting solar-driven nitrogen fixation in pure water. Adv. Mater., 2017, 29 1701774.
[12] Y. Zhao, Y. Zhao, R. Shi, B. Wang, G. Waterhouse, L. Wu, C. Tung, T. Zhang, Tuning oxygen vacancies in ultrathin TiO_2 nanosheets to boost photocatalytic nitrogen fixation up to 700 nm, Adv. Mater., 2019, 31, 1806482.
[13] N. Zhang, A. Jalil, D. Wu, S. Chen, Y. Liu, C. Gao, W. Ye, Z. Qi, H. Ju, C. Wang, X. Wu, L. Song, J. Zhu, Y. Xiong, Refining defect states in $W_{18}O_{49}$ by Mo doping: A strategy for tuning N_2 activation towards solar-driven nitrogen fixation, J. Am. Chem. Soc., 2018, 140, 9434-9443.
[14] Q. Li, Y. Shi, Z. Wang, C. Liu, J. Bi, J. Yu, L. Wu, Nitrogen activation and surface charge regulation for enhancing the visible-light-driven N_2 fixation over MoS_2/UiO-66$(SH)_2$, J. Colloid Interface Sci., 2023, 652, 1568-1577.
[15] T. He, Z. Zhao, R. Liu, X. Liu, B. Ni, Y. Wei, Y. Wu, W. Yuan, H. Peng, Z. Jiang, Y. Zhao, Porphyrin-based covalent organic frameworks anchoring Au single atoms for photocatalytic nitrogen fixation, J. Am. Chem. Soc., 2023, 145, 6057-6066.
[16] N. Kwon, J. Park, X. Jin, S. Kim, H. Kim, S. Hwang, Defect-regulated two-dimensional superlattice of holey g-C_3N_4-TiO_2 nanohybrids: Contrasting influence of vacancy content on hybridization impact and photocatalyst performance, ACS Nano, 2023, 17, 23732-23745.
[17] Y. Peng, A. Melillo, R. Shi, A. Forneli, A. Franconetti, J. Albero, H. García, Light-assistance in nitrogen fixation to ammonia by highly dispersed Cs-promoted Ru clusters supported on ZrO_2, Appl. Catal. B: Environ., 339 (2023) 123143.